



Highly flexible O,O',N ligands and their Fe, Ni, Cu and Zn complexes

Katharina Butsch^a, Axel Klein^{a,*}, Matthias Bauer^b

^a Universität zu Köln, Department für Chemie, Institut für Anorganische Chemie, Greinstrasse 6, D-50939 Köln, Germany

^b Karlsruhe Institut of Technology (KIT), Institut für Technische Chemie und Polymerchemie, Engesserstr. 20, D-76131 Karlsruhe, Germany

ARTICLE INFO

Article history:

Available online 3 March 2011

Dedicated to Wolfgang Kaim on the occasion of his 60th birthday.

Keywords:

Oxido-pincer ligands (O,O,N ligands)

Iron(III)

Nickel(II)

Copper(II)

Zinc(II)

EPR spectroscopy

ABSTRACT

Three new chiral ligands bearing an O,O',N donor set (O_{methoxy}O_{hydroxy}N_{pyridine}) were synthesised and coordinated to Fe^{III}, Fe^{II}, Ni^{II}, Cu^{II} and Zn^{II} to yield complexes with the general formula [M(OON)Cl_x]_y. While the pyridine N and the hydroxy O atoms coordinate strongly to all applied metal ions, the methoxy donor seems not to be involved in coordination, although some evidence for a weak interaction between O_{Me} and the Zn^{II} were found in NMR spectra. In the bidentate O',N coordination mode the new ligands exhibit several coordination geometries as analysed in the solid compounds by XRD, EXAFS and EPR and in solution by UV–Vis absorption, cyclic voltammetry, EXAFS, EPR or NMR spectroscopy.

© 2011 Elsevier B.V. All rights reserved.

1. Introduction

Ligands bearing a tridentate O,E,O donor set where E = C, N, P etc. are well known. The most common, called oxido-pincer ligands, contain an aromatic central core and two pendant arms carrying various oxygen donor functions. Most important are ligands with a central pyridine ring, which have found a number of applications, e.g. in catalysis [1]. Typical oxido donor functions can be carboxylates [2], carbonyl [3] or alcohol functions [4]. The latter are most interesting, since they provide the opportunity of step-wise deprotonation upon coordination which leads to a large diversity of complexes and structures. An increasing tendency to deprotonation is expected with increasing hardness (HSAB) of the metal ion. Consequently, complexes of early transition metals (groups 4–6) exclusively contain the fully deprotonated ligand dianions [5]. Intermediate cases (partly deprotonated) were found in polynuclear manganese complexes [6], while late transition metals (groups 9–12) usually coordinate to the fully protonated ligands [4a,7]. However, there are also exceptions from this correlation, e.g. as found in [Cu₂(η²,μ-pydimH)₂(η³-pydimH₂)₂]²⁺ [7d,8] and in [Cu(pydimH₂)(pydimH)]⁺ [7d]

In agreement with the HSAB concept [9], weak bonds are observed between the O-donor functions and late transition metal ions like Co^{II}, Ni^{II}, Cu^{II} and Zn^{II}, while the metal ions Pd^{II} and Pt^{II}

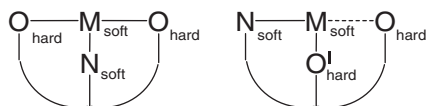
exclusively bind to the pyridine nitrogen [10,11]. As a result, oxido-pincer ligands show a wealth of structural motifs including square planar (Pt, Pd), trigonal-bipyramidal (Co, Ni, Zn), square pyramidal (Cu) and octahedral (Co, Ni, Cu, Zn) coordination [10,12,13].

Most of the studies reported so far focus on symmetric oxido-pincer ligands with an O,N,O donor set. The modification of the donor atom sequence from O,N,O to O,O,N or O,O',N (Scheme 1) gives some interesting possibilities because of the intrinsic asymmetry and the option to build up hemilabile systems resulting from the *trans*-effect of the (presumably) strong N–M interaction which weakens the peripheral M–O bond.

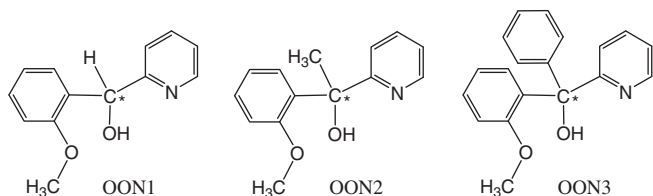
In this contribution three new chiral O,O',N pincer ligands were synthesised (Scheme 2). The new ligands were designed focussing on four main aspects. (i) Compared to the frequently used oxido-pincer ligands with a central pyridine core and two pendant carboxylate or methanol functions, the new ligands provide not only a change in donor atom sequence O,N,O → O,O',N but also an altered sequence of (expected) binding strength O_{weak}N_{strong}, O_{weak} → O_{weak}O'_{weak}N_{strong} towards soft metal ions as indicated in Scheme 1. (ii) The ligands provide the possibility of tris-chelate binding, upon forming two five-membered chelate rings. In contrast to ligands containing rigid aromatic cores such as pyridine which allow only η³-*meridional* binding, here the central binding position is far more flexible and might open the option of a η³-*facial* binding. The steric bulk at the central C atom increases within the series OON1 < OON2 < OON3, while the acidity of the hydroxy function is expected to decrease along the series OON3 > OON1 > OON2. (iii) Only one of the two oxido donor functions

* Corresponding author.

E-mail address: axel.klein@uni-koeln.de (A. Klein).



Scheme 1. Schematic binding situation of O,N,O oxido-pincer ligands compared to O,O',N ligands to soft transition metal ions.



Scheme 2. The new chiral O,O',N pincer-ligands; left: 2-(hydroxy(pyridin-2-yl)methyl)methoxyphenol (OON1), middle: 2-(1-hydroxy-1-(pyridin-2-yl)ethyl)phenol (OON2), right: 2-(hydroxy(phenyl)(pyridin-2-yl)methyl)phenol (OON3).

can be deprotonated upon coordination, since the second is a methoxy group. The methoxy and hydroxyl functions are expected to exert approximately the same binding strength but deprotonation of the central hydroxyl group will greatly enhance its coordination capacity over that of the methoxy group (creating a $O_{\text{weak}}, O'_{\text{strong}}, N_{\text{strong}}$ binding situation). (iv) The new ligands are chiral due to four different substituents at the central C atom. The chiral centre is very close to the metal atom, which might be important for the transfer of chiral information to a substrate bound at the central metal ion.

The three ligands were reacted with precursors containing Fe^{III} , Ni^{II} , Cu^{II} and Zn^{II} . These metal ions are expected to increase in “hardness” along the series $\text{Cu}^{\text{II}} < \text{Ni}^{\text{II}} < \text{Fe}^{\text{III}}$ and also provide different preferences for coordination polyhedra. The structures of the new complexes in the solid were studied by a combination of XRD on single crystals, and EXAFS and EPR spectroscopy on powders of selected compounds (focussing on Cu^{II} and Fe^{III}). The structures in solution were investigated using UV–Vis absorption spectroscopy, and in the case of the diamagnetic Zn^{II} compounds additionally by ^1H NMR. The paramagnetic Cu^{II} and Fe^{III} complexes were investigated by EPR spectroscopy, and all complexes have been submitted to electrochemical experiments (mainly cyclic voltammetry).

2. Results and discussion

2.1. Preparation and structure of the ligands

The ligands were synthesised by Grignard coupling reaction of 2-iodo-anisole with 2-formylpyridine (OON1), 2-acetylpyridine (OON2), or 2-benzoylpyridine (OON3), respectively. The resulting ligands were obtained as racemates and characterised by NMR and elemental analysis. All ligands were used as racemates for complex synthesis and characterisation. The ligands exhibit a good solubility in organic solvents and were purified by recrystallisation from acetone, upon which single crystals of OON2 and OON3 were obtained and analysed by XRD (details in the [Supplementary material](#)). In the molecular structures of the free ligands the O,O',N binding pocket is not available, however, the coordinating sites (O,O',N) are arranged around the central chiral C atom in a rather flexible way and the conformational changes necessary to allow tridentate facial coordination are probably very small.

2.2. Preparation of the complexes

The complexes were obtained by stirring the metal chloride salts with the ligands in a 1:1 ratio at 298 K in methanol for 16 h, without the use of external base. Strongly coloured products of the general formulae $[\text{M}^{\text{II}}(\text{O},\text{O}',\text{N})\text{Cl}_2]$ ($\text{M} = \text{Ni}, \text{Cu}, \text{Zn}$) or $[\text{Fe}^{\text{III}}(\text{O},\text{O}',\text{N})\text{Cl}_3]$ (except OON2) were obtained in high yields. While the Ni, Cu and Zn compounds (despite $[\text{Cu}(\text{OON1})\text{Cl}_2]_n$) show good solubility in polar organic solvents such as acetone, methanol, ethanol, THF, DMF or MeCN, the Fe compounds are less soluble. Several attempts to obtain the Fe^{III} complex $[\text{Fe}(\text{OON2})\text{Cl}_3]$ failed – in all cases virtually insoluble orange material was obtained which gave elemental analyses far from a reasonable stoichiometry (see Section 4). The iron complexes $[\text{Fe}(\text{OON1})\text{Cl}_3]$ and $[\text{Fe}(\text{OON3})\text{Cl}_3]$ require strongly polar solvents such as MeCN or DMF to be dissolved.

2.3. Crystal and molecular structures from XRD

From the compounds $[\text{Fe}(\text{OON1})\text{Cl}_2]_2$, $[\text{Cu}(\text{OON1})\text{Cl}_2]_n$ and $[\text{Cu}(\text{OON3})\text{Cl}_2]_2$ single crystals were obtained which could be analysed by X-ray diffraction. Details of the structures are shown in [Figs. 1–3](#), essential crystal and structural data is collected in the [Supplementary material](#).

When recrystallising the complex $[\text{Fe}(\text{OON1})\text{Cl}_3]$ from acetone solution, single crystals of the dimeric complex $[\text{Fe}(\text{OON1})\text{Cl}_2]_2$ were obtained (see [Fig. 1](#)). The compound has obviously been formed through elimination of HCl (Eq. (1))



The crystal structure was solved and refined in the triclinic space group $P\bar{1}$ ([Tables 1](#), and [Supplementary material](#)). In the crystal structure the two iron atoms are bridged by the central deprotonated oxido function of the OON1 ligand, forming a polyhedron of two edge-sharing (distorted) trigonal bipyramids with a nearly planar Fe_2O_2 core (with a dihedral angle Fe1-O1-Fe2-O2 of $9.8(2)^\circ$ and small O–Fe–O angles of $73.31(2)^\circ$ and $73.12(2)^\circ$). The trigonal planes around Fe^{III} are formed by the two chlorido ligands and one of the bridging O atoms. The axial positions are occupied by the pyridine N atoms and the second bridging O atom,

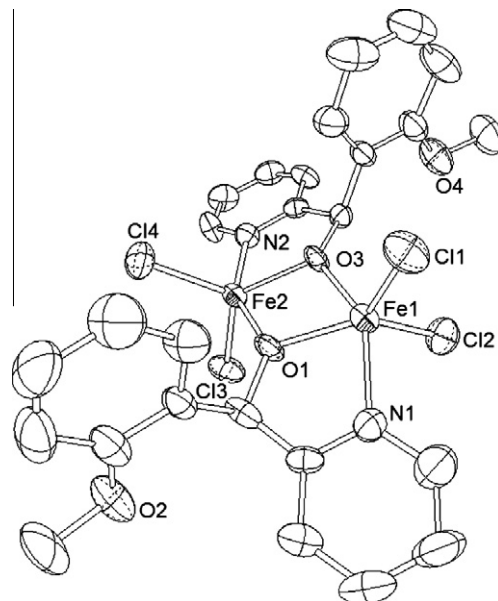


Fig. 1. ORTEP representation (with 50% probability ellipsoids) of the molecular structure of $[\text{Fe}(\text{OON1})\text{Cl}_2]_2$, hydrogen atoms are omitted for clarity.

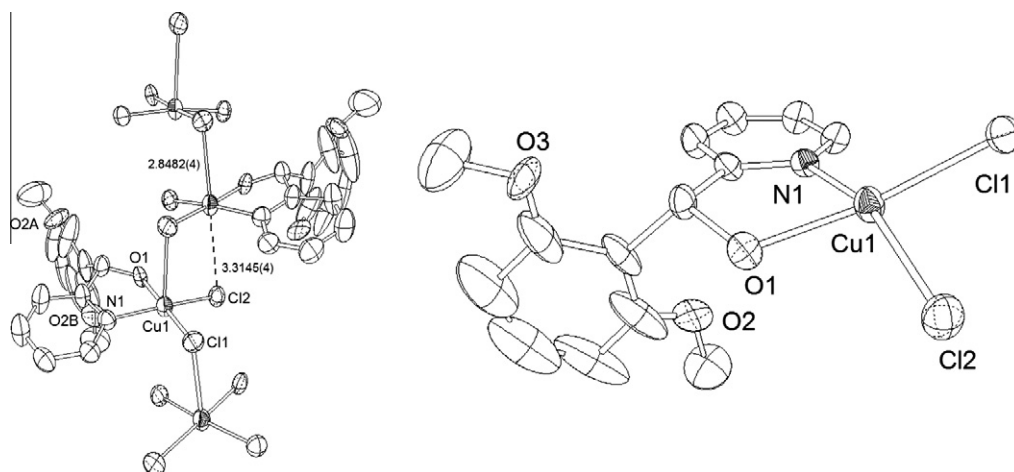


Fig. 2. View on the polymeric chain structure of $[\text{Cu}(\text{OON1})\text{Cl}_2]_n$ (30% probability level) (left); ORTEP representation of the asymmetric unit in the chain structure with the disordered anisole ring (right); H atoms are omitted for clarity in both figures.

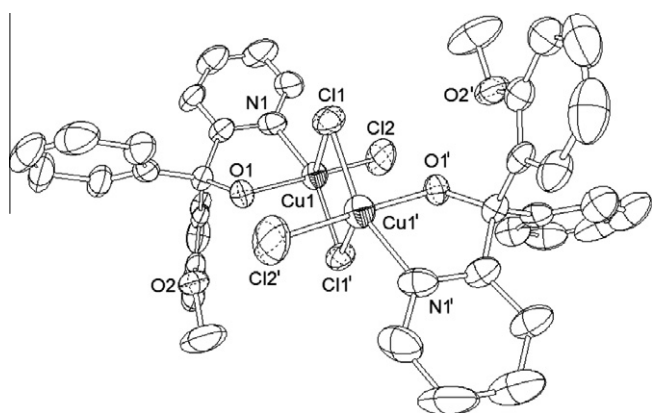


Fig. 3. ORTEP representation (with 50% probability ellipsoids) of the molecular structure of $[\text{Cu}(\text{OON3})\text{Cl}_2]_2$, hydrogen atoms are omitted for clarity.

the angles N1-Fe1-O3 ($147.0(2)^\circ$) and N2-Fe2-O1 ($150.1(2)^\circ$) deviate markedly from the ideal angle of 180° . The methoxy function remains uncoordinated. Interestingly, the dimer is formed by two mononuclear units which contain ligands of the same chirality; one of the molecules in the unit cell possesses ligands of *R* configuration, this is depicted in Fig. 1, the other molecule possesses ligands of *S* chirality, thus in the crystal structure both types of stereoisomers occur.

The Cu^{II} compound $[\text{Cu}(\text{OON1})\text{Cl}_2]_n$ was crystallised from acetone solution and the structure was solved and refined in the monoclinic space group $P2_1/c$ (Tables 1 and Supplementary material). The structure (Fig. 2) shows a one-dimensional stack of square planar coordination units consisting of Cu^{II} , with an η^2 -N,O bound OON1 ligand and two Cl ligands, connected along the crystallographic *c* axis by rather long axial Cl–Cu bonds (using one of the Cl ligands). While the Cu–Cl bond in the apical position is $2.848(2)$ Å, the Cu–Cl distance opposite is $3.144(4)$ Å (Fig. 2). Although this is a rather long Cu–Cl distance, similar [14,15] or even longer distances (about 3.5 Å) [16] have been found for chloride bridged dimers. The overall geometry around the Cu atom is thus square pyramidal (or asymmetrically elongated octahedral). Similar to the Fe^{III} complex, OON1 coordinates in a bidentate mode to the CuCl_2 fragment and a 50% disorder of the methoxy groups was found. The OON1 ligands alternate in the chain structure so that all ligands on one side of the chain possess the same chirality.

The Cu^{II} compound $[\text{Cu}(\text{OON3})\text{Cl}_2]_2$ was crystallised from acetone and the structure was solved and refined in the monoclinic

Table 1
Selected distances and angles of $[\text{FeCl}_2(\text{OON1})]_2$ and $[\text{CuCl}_2(\text{OON1})]_n$.

Distances (Å)	Distances (Å)	Angles ($^\circ$)			
<i>[Fe(OON1)₂Cl₂]</i>					
Fe1–O1	1.951(4)	Fe1–Cl2	2.212(2)	O1–Fe1–O3	73.3(1)
Fe2–O1	1.981(3)	Fe2–Cl4	2.176(2)	O1–Fe2–O3	73.2(1)
Fe1–Cl1	2.173(2)	Fe2–N2	2.088(4)	Cl1–Fe1–Cl2	111.45(9)
Fe2–Cl3	2.223(2)	O1...O3	2.350(1)	Cl3–Fe2–Cl4	112.79(9)
Fe1–N1	2.109(5)	Fe1...Fe2	3.147(1)	N1–Fe1–O3	147.0(2)
Fe1–O3	1.986(3)	Fe1...OMe	4.994(2)	N2–Fe2–O1	150.1(2)
Fe2–O3	1.965(4)	Fe2...OMe	4.931(2)	N1–Fe1–Cl1	99.2(1)
				N2–Fe2–Cl3	95.2(1)
<i>[Cu(OON1)Cl₂]_n</i>					
Distances (Å)		Angles ($^\circ$)			
Cu1...OMe	4.089(4)				

space group $P2_1/c$ (Tables 2 and Supplementary material). The structure shows a binuclear $\mu\text{-Cl}_2$ -bridged complex entity (see Fig. 3). The crystal structure reveals a short intramolecular H bridge between O2 and H1 with a distance of $1.94(5)$ Å. Furthermore, intermolecular π stacking along the crystallographic *a* axis is observed for the anisole rings of neighbouring molecules. The two rings are coplanar ($0.00(3)^\circ$) and exhibit a rather short interplanar distance ($3.53(2)$ Å). In the binuclear $[\text{Cu}(\text{OON3})\text{Cl}_2]_2$ molecules, the Cu^{II} ions (see Fig. 3) are coordinated by the N and O atoms of the OON3 ligands, one peripheral chlorido ligand and two bridging chlorido ligands. The resulting coordination polyhedron can be described as distorted square-pyramidal with the $\mu\text{-Cl}$ (Cl1) atom in the axial positions or as distorted trigonal-bipyramidal with N1 and Cl1' as axial ligands. The two OON3 ligands which are part of the binuclear molecule reveal opposite chirality, in contrast to the iron complex. Again, the methoxy group is non-coordinating ($\text{Cu}\cdots\text{OMe} = 4.121(2)$ Å).

2.4. Structure determination using XAS

Since single crystals were not obtained for most of the new compounds we embarked on a XAS study of selected compounds. The edge position and the weak signal at around 8.977 keV in the

Table 2
Angles found for [Cu(OON3)Cl₂]₂ compared to angles of ideal coordination polyhedra.

Angles	Found (°)	TBP-ideal (°)	TPy-ideal (°)
O1–Cu1–Cl2	171.23(1)	120	180
O1–Cu1–Cl1	85.42(1)	120	90
Cl2–Cu1–Cl1	102.07(1)	120	90
Σa ^a	358.06(2)		360
Σb ^b	358.72(1)	360	

^a Σa = (N1–Cu1–O1) + (N1–Cu1–Cl2) + (Cl1–Cu1–O1) + (Cl1–Cu1–Cl1).

^b Σb = (O1–Cu1–Cl2) + (O1–Cu1–Cl1) + (Cl2–Cu1–Cl1).

copper spectra indicates an oxidation state of Cu^{II}. The rather high pre-peak intensity in the iron spectra is in accordance with the fivefold coordination.

The XANES spectra of the copper and iron samples are given in Fig. S4. For both metals, all the samples look similar to each other, i.e. no significant changes in the nearest neighbour contributions are found, hence we assume the same O/N and Cl shells as for the examples where XRD-structures were obtained. Since oxygen and nitrogen can not be distinguished due to their similar amplitude and phase functions, they are grouped in one backscattering contribution in the EXAFS analysis (see Table 3 and Supplementary material). Only the metal...carbon coordination numbers were

iterated as a cross check, because the obtained coordination numbers should agree with the XRD structures if the models used to fit the EXAFS data are correct. In all cases, the M–C number is in good agreement with the XRD values.

The Cu/Fe–O/N and Cu/Fe–C distances from the EXAFS measurements are in all cases in good agreement with the XRD structures. While in the case of [Cu(OON1)Cl₂]_n the adjustment of one copper-backscatterer decreased the R-factor slightly, the R-factor was slightly increased on introducing a Cu shell to the dimeric [Cu(OON3)Cl₂]₂. Thus the assignment of [Cu(OON2)Cl₂]₂ having a dimeric nature with a short Cu...Cu distance of about 3.2 Å seems to be justified, the fit in this case was also slightly better after the incorporation of a Cu shell.

An Fe...Fe contribution was found for [Fe(OON1)Cl₂]₂; the Fe...Fe distance agrees well with the XRD value. On the other hand, in [Fe(OON1)Cl₃] and [Fe(OON3)Cl₃] no Fe...Fe interaction was found, pointing to five-coordinated monomeric complex species. The EXAFS spectra are supplied in the Supplementary material.

2.5. EPR spectroscopy of Cu^{II} and Fe^{III} compounds

For the Cu^{II} and Fe^{III} compounds EPR spectra were measured at 298 K on powder samples and solutions (data collected in Table 4).

Table 3
EXAFS parameters determined for copper and iron complexes.

Sample	Abs-Bs	N(Abs)	Distance (XRD) (Å)	R(Abs-Bs) (Å)	σ (Å ²)	R (%)
[Cu(OON1)Cl ₂] _n	Cu–N/O	2	1.9863(3)/2.0016(2)	1.99 ± 0.02	0.008 ± 0.001	10.5
	Cu–Cl	3	2.2494(3)/2.2549(3)/2.8481(4)	2.24 ± 0.02	0.009 ± 0.001	
	Cu–C	2.8 ± 0.6		2.90 ± 0.03	0.022 ± 0.004	
	Cu–Cu	1	3.8146(4)	3.83 ± 0.04	0.025 ± 0.005	
[Cu(OON2)Cl ₂] ₂	Cu–N/O	2		1.97 ± 0.02	0.019 ± 0.002	15.07
	Cu–Cl	3		2.20 ± 0.02	0.020 ± 0.002	
	Cu–C	2.1 ± 0.4		2.88 ± 0.03	0.012 ± 0.002	
	Cu–Cu	1		3.32 ± 0.03	0.025 ± 0.005	
[Cu(OON3)Cl ₂] ₂	Cu–N/O	2	1.9951(7)/2.0024(5)	1.99 ± 0.02	0.024 ± 0.002	14.11
	Cu–Cl	3	2.2676(6)/2.647(1)/2.2057(9)	2.21 ± 0.02	0.016 ± 0.002	
	Cu–C	2.4 ± 0.5		2.89 ± 0.03	0.014 ± 0.003	
	Cu–Cu	1	3.268(1)	3.31 ± 0.03	0.025 ± 0.005	
[Fe(OON1)Cl ₂] ₂	Fe–N/O	3	1.9852(7)/1.9507(7)/2.1072(6)	1.97 ± 0.02	0.013 ± 0.001	6.67
	Fe–Cl	2	2.1741(7)/2.213(1)	2.20 ± 0.02	0.007 ± 0.001	
	Fe–C	1.8 ± 0.4		2.96 ± 0.03	0.002 ± 0.001	
	Fe–Fe	1	3.1467(9)	3.12 ± 0.03	0.011 ± 0.002	
[Fe(OON1)Cl ₃]	Fe–N/O	2		1.98 ± 0.02	0.025 ± 0.003	15.99
	Fe–Cl	3		2.19 ± 0.02	0.012 ± 0.002	
	Fe–C	3.4 ± 0.7		2.99 ± 0.03	0.025 ± 0.005	
[Fe(OON3)Cl ₃]	Fe–N/O	3		1.99 ± 0.02	0.014 ± 0.003	12.55
	Fe–Cl	2		2.21 ± 0.02	0.005 ± 0.001	
	Fe–C	2.9 ± 0.6		3.04 ± 0.03	0.025 ± 0.005	

Table 4
X-band EPR data of Cu^{II} and Fe^{III} complexes.^a

Sample	State	g _{av}	g ₁ or g	g ₂ or g _⊥	g ₃	Δg	Geometry ^b
[Cu(OON1)Cl ₂]	amorphous	2.148	2.267	2.128	2.048	0.219	OE or Spy
[Cu(OON1)Cl ₂] _n	polycryst.	2.148	2.286	2.079	-	0.207	OE or Spy
[Cu(OON1)Cl ₂]	dissolved ^c	2.128	2.207	2.128	2.050	0.157	OE
[Cu(OON2)Cl ₂]	amorphous	2.145	2.247	2.134	2.053	0.194	OE or Spy
[Cu(OON2)Cl ₂]	dissolved ^c	2.128	2.210	2.127	2.048	0.162	OE
[Cu(OON3)Cl ₂]	amorphous	2.145	2.283	2.076	-	0.207	OE or Spy
[Cu(OON3)Cl ₂]	dissolved ^c	2.131	2.209	2.130	2.054	0.155	OE
[Fe(OON1)Cl ₃]	amorphous	2.024		2.024			TBP or OE
[Fe(OON1)Cl ₂] ₂	polycryst.	2.063	2.723	2.052	1.414	1.309	TBP
[Fe(OON3)Cl ₃]	amorphous	2.212	3.081	2.048	1.508	1.573	TBP or OE

^a Cu^{II} and Fe^{III} measured at 298 K; averaged g value g_{av} = (g_{||} + 2g_⊥)/3 or g_{av} = (g₁ + g₂ + g₃)/3; g anisotropy Δg = g_⊥ – g_{||} or Δg = g₁ – g₃.

^b Symmetry assigned by XRD or assumed from EPR spectroscopy; SPY = square pyramidal, TBP = trigonal bipyramidal, OE = octahedral elongated.

^c Dissolved in an acetone/THF (1:1) mixture.

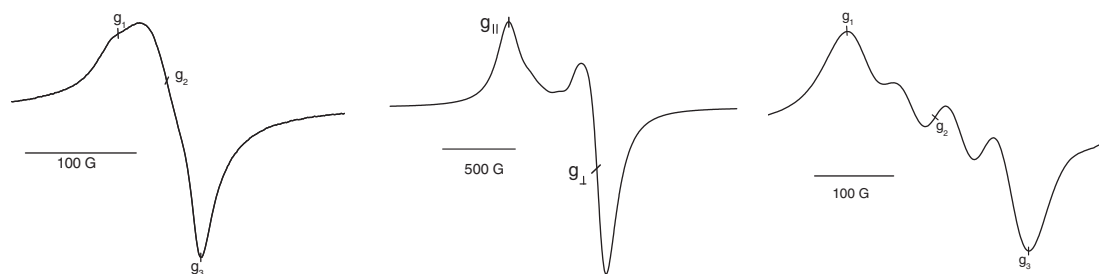


Fig. 4. X-band EPR spectra of an amorphous powder of $[\text{Cu}(\text{OON1})\text{Cl}_2]$ (left), polycrystalline powder of $[\text{Cu}(\text{OON1})\text{Cl}_2]_n$ (middle) and $[\text{Cu}(\text{OON1})\text{Cl}_2]$ in acetone/THF (1:1) (right); samples measured at 298 K.

Fig. 4 shows EPR spectra recorded for the amorphous material obtained from the preparation procedure $[\text{Cu}(\text{OON1})\text{Cl}_2]$ (parent material), the recrystallised and structurally characterised binuclear complex $[\text{Cu}(\text{OON1})\text{Cl}_2]_n$ and an acetone/THF solution of the parent material. While the spectra of the parent material $[\text{Cu}(\text{OON1})\text{Cl}_2]$ and its solution show rhombic symmetry, the polymeric compound exhibits an axial EPR signal with $g_{||} > g_{\perp}$ (see Table 4).

The latter signal shape is in line with the elongated square pyramidal (octahedral) coordination revealed from XRD. The rhombic symmetry of the other two spectra indicates distorted square-pyramidal coordination as found in the recently described complex $[(\text{pydimH}_2)\text{CuCl}_2]$ ($g_{av} = 2.149$, $g_1 = 2.311$, $g_2 = 2.094$, $g_3 = 2.041$, $\Delta g = 0.270$) [13]. From the similarity of the average g value and the g anisotropy (Δg) of the parent compound and $[(\text{pydimH}_2)\text{CuCl}_2]$ we conclude that in both compounds the ligand binds in a tridentate fashion. From the significantly different values from the solution spectrum it can be concluded that the binding situation has changed markedly upon dissolving the parent compound. We assume a square pyramidal coordination sphere with a N,O' bidentate binding mode and a solvent molecule binding to Cu, in line with the findings from NMR spectroscopy of the corresponding Zn^{II} complexes (see later). This is true for all three Cu complexes.

The spectra of the iron complexes $[\text{Fe}(\text{OON1})\text{Cl}_3]$ (parent material) and $[\text{Fe}(\text{OON1})\text{Cl}_2]_2$ (recrystallised) are not identical. The parent material exhibits a broad isotropic EPR signal with a g value of 2.024 ($\Delta H \sim 3000$ G) and a half-field signal at $g = 4.305$. In contrast to this, the binuclear species reveals a rhombic spectrum with a smaller g value ($g_{av} = 2.063$) and a Δg of 1.309. The spectrum of amorphous $[\text{Fe}(\text{OON3})\text{Cl}_3]$ also has rhombic symmetry but higher g values and Δg . The total spectral width of all three spectra is very similar and importantly, the low g values of all complexes are in line with a Fe^{III} low-spin configuration [17]. Dissolving the two parent amorphous Fe^{III} complexes in an acetone/THF mixture leads in both cases to isotropic, narrow ($\Delta H \sim 60$ G) EPR spectra with a g value of 2.014. So far we could not assign this species.

2.6. NMR and UV-Vis spectroscopy in solution

From the Zn^{II} compounds (d^{10} diamagnetic) NMR spectra could be obtained. Table 5 lists selected data (for complete data see Section 4). Special attention was paid to the chemical shifts of the OH, OCH_3 and H6_{py} atoms since they are most sensitive to coordination of the metal to the adjacent donor atoms. Since this coordination might depend on the solvent polarity and/or the solvent's ability to act as a ligand, spectra were recorded in CDCl_3 (unpolar, non-coordinating), $[\text{D}_6]$ -acetone (polar, presumably non-coordinating), $[\text{D}_4]$ -methanol (highly polar, potentially coordinating), $[\text{D}_5]$ -pyridine and $[\text{D}_7]$ -DMF (both polar, presumably coordinating).

Upon coordination signals of the protons adjacent to donor atoms usually exhibit a low-field shift. In CDCl_3 these shifts are

Table 5
Selected NMR data for free OON ligands and Zn^{II} complexes.^a

In CDCl_3	$\delta \text{H6}_{\text{py}}$	$\Delta\delta$	δOH	$\Delta\delta$	δOMe	$\Delta\delta$
OON1	8.54		5.20		3.86	
$[\text{ZnCl}_2(\text{OON1})]$	8.71	0.17	7.30	2.10	3.75	0.11
OON2	8.49		5.12		3.56	
$[\text{ZnCl}_2(\text{OON2})]$	8.73	0.24	6.55	1.43	3.71	0.15
OON3	8.55		5.71		3.53	
$[\text{ZnCl}_2(\text{OON3})]$	8.74	0.19	7.72	2.01	3.81	0.28
In $[\text{D}_6]$ -acetone						
OON1	8.50		5.33		3.83	
$[\text{ZnCl}_2(\text{OON1})]$	8.76	0.26	8.77	3.44	3.84	0.01
OON2	8.42		5.10		3.55	
$[\text{ZnCl}_2(\text{OON2})]$	8.70	0.28	7.94	2.84	3.49	0.06
OON3	8.46		5.67		3.49	
$[\text{ZnCl}_2(\text{OON3})]$	8.73	0.27	8.18	2.51	3.66	0.17
In $[\text{D}_7]$ -DMF						
OON3	8.56		6.03		3.56	
$[\text{ZnCl}_2(\text{OON3})]$	8.58	0.02	6.16	0.13	3.57	0.01

^a Chemical shifts δ in ppm vs. TMS. Change of the chemical shift $\Delta\delta$ upon coordination in ppm.

relatively small for the H6_{py} atom and the OMe group ($\Delta\delta = 0.1$ – 0.28 ppm) but large for the OH group (1.4–2.1 ppm). In $[\text{D}_6]$ -acetone the $\Delta\delta$ values for the H6_{py} and OH protons point to coordination, while the $\Delta\delta$ values for the OMe group for the complexes with OON1 and OON2 drop to zero (indicating non-coordination). Qualitatively the same holds for $[\text{Zn}(\text{OON3})\text{Cl}_2]$ in $[\text{D}_4]$ -methanol, although the OMe proton signal overlaps with the signal of the solvent protons and thus cannot be studied. Importantly, the OH proton of the ligands can be unequivocally detected, thus the ligands remain protonated upon coordination. In the coordinating solvents $[\text{D}_7]$ -DMF and $[\text{D}_5]$ -pyridine, the $\Delta\delta$ values strongly indicate that the OON ligands were replaced by solvent molecules; the shift observed for the OH proton might also be due to H bridge formation with solvent molecules.

For the Ni^{II} complexes the ^1H NMR spectra show paramagnetic broadening, meaning that 2D experiments failed and no assignments of the signals could be made. Tetrahedral or (distorted) octahedral configurations can be assumed from the observed paramagnetism. This is in contrast to recently reported Ni complexes of oxido-pincer ligands with phenolate groups [2,6-bis(2-methoxyphenyl)pyridine (LOMe_2), 2,6-bis(2-hydroxyphenyl)pyridine (LOH_2), 2,6-bis-(2,4-dimethoxyphenyl)pyridine (LOMe_4)] which were diamagnetic, bromido bridged dimers [12].

UV-Vis absorption spectra were recorded in the range 200–1000 nm (figures and data collected in the [Supplementary material](#)). The absorption spectra of all complexes show intense absorption bands in the UV range (λ_1), which can be assigned to π - π^* transitions within the ligands. As expected, the Zn complexes do not show any further absorptions. Interestingly, the three iron complexes exhibit quite similar absorption spectra indicating that

Fe^{III} is still coordinated, in line with the EPR experiments. In addition to the π - π^* absorption bands the iron and the copper complexes show bands in the range 300–400 nm. Based on their intensities and their negative solvatochromism these bands were assigned in both cases to halide-to-metal charge transfer (LMCT) transitions. Within the series of experiments to determine the solvatochromism, ligand de-coordination was observed for the copper complexes for some solvents. In MeOH and EtOH solution correlation of the LMCT energy with typical solvent parameters as the Dimroth–Reichardt parameter (E_T) [18] fails, probably due to the protic character of these solvents (for details see [Supplementary material](#)). While the iron complexes do not exhibit further bands, for the copper and nickel complexes long-wavelength d–d (ligand field) absorptions were observed in the visible range. For the copper complexes it could be noted that the spectra of DMF solutions differ markedly from spectra in other solvents indicating a de-coordination of the OON ligands, in line with the NMR results obtained for the zinc complexes. The long-wavelength bands of the nickel complexes clearly show d–d bands typical for an octahedral coordination around Ni^{II} giving proof for the binuclear character of these complexes.

2.7. Electrochemical and spectroelectrochemical investigations

Cyclic voltammetry was measured on the free ligands and the new Cu, Fe and Ni complexes (Table 6). Surprisingly, the first reduction of the ligands OON2 and OON3 was found to be fully reversible, while the corresponding reduction wave for OON1 lies far more negative and is irreversible. A UV–Vis spectroelectrochemical experiment confirmed that even under these conditions (several minutes) the processes for OON2 and OON3 were reversible (for Details see [Supplementary material](#)). The isotropic EPR spectrum of the reduced species generated from OON3 using K/cryptand [2.2.2] showed a three line pattern at $g = 2.0034$ (figure and simulation in the [Supplementary material](#)). The best simulation assumed two ¹H nuclei coupling to the unpaired electron with $a_H = 2.1$ G. Comparison of the redox potentials of the three ligands shows that variation of the residue (H, CH₃, Ph) highly influences the first reduction potential of the O,O',N ligands and the stability of the corresponding radicals. More importantly, for the corresponding Fe^{III}, Ni^{II}, Cu^{II} and Zn^{II} complexes no such reversible ligand-centred reduction can be observed. In these complexes ligand-centred reductions occur irreversibly and at very negative potentials (as for OON1). This has led us to the assumption that a specific geometry is required to stabilise the corresponding radicals, which is not the case for OON1 and the coordinated ligands OON2 and OON3. The small coupling constants and the absence of (or very small) coupling to the ¹⁴N nucleus let us assume that

both the anisole and the pyridine ring contribute to the singly occupied molecular orbital. The stabilisation of these radicals might thus be similar as for triphenyl-methyl radicals and derivatives [19]. Of course, more detailed investigations including quantum chemical calculations, detailed spectroelectrochemical EPR and UV–Vis experiments and further derivatives are necessary to provide evidence for this effect.

For the copper complexes reversible Cu^{II}/Cu^I redox couples were found around 0 V indicating high flexibility of the coordination polyhedra. The three ligands do not influence the redox potentials markedly. This is in line with the EPR experiments, which already revealed that the Cu^{II} ions in the three complexes are magnetically (and thus structurally) identical in solution (Table 6). Further reductions (presumably ligand-centred) and oxidations occur irreversibly at potentials around –2 and 1 V, respectively (for details see [Supplementary material](#)).

The two iron complexes [Fe(OON1)Cl₃] and [Fe(OON3)Cl₃] show reduction waves corresponding to the Fe^{III}/Fe^{II} couple. To establish the fully reversible character of these redox couples we synthesised the corresponding Fe^{II} complexes (including the OON2 derivative, see Section 4) and found reversible oxidation waves at the same potentials. Unfortunately, these three Fe^{II} compounds are virtually insoluble, largely hampering further characterisation. For the binuclear Fe^{III} complex [Fe(OON1)Cl₂]₂ a reversible reduction wave was detected at far lower potentials, basically in line with the increased ligand-strength of the central O donor atom upon deprotonation (OH → O[–]).

The nickel complexes cannot be oxidised in a range between 0.0 and 2.0 V, and irreversible reductions were observed around –1.8 V. They were assigned to Ni^{II}/Ni^I reduction followed either by splitting of chlorido ligands or disproportionation to Ni^{II} and Ni⁰. In both cases disintegration of the complexes will result and indeed only the free ligands could be detected (by NMR) in electrolysed solutions.

3. Conclusion

The chiral ligands with O,O',N donor sets presented here successfully coordinate to the metal ions Zn^{II}, Cu^{II}, Ni^{II} and Fe^{III}. Single crystals of [Fe(OON1)Cl₂]₂, [Cu(OON1)Cl₂]_n and [Cu(OON3)Cl₂]₂ were obtained and analysed by X-ray diffraction. EXAFS investigations reveal that these compounds were not the primary products from the synthesis procedures but result from recrystallisation. The primary products were mononuclear for Cu^{II} [Cu(O,O',N)Cl₂], and Fe^{III} [Fe(O,O',N)Cl₃]. For the Zn^{II} derivatives [Zn(O,O',N)Cl₂] the excellent solubility points to a mononuclear character, while the very low solubility and NMR spectra of the Ni^{II} derivatives points to binuclear complexes [Ni(O,O',N)Cl₂]₂ with chlorido-bridged, octahedrally configured Ni^{II}. In the solid structures (XRD and EXAFS) and in solutions of coordinating solvents (as DMF, THF or pyridine) the ligands were N,O' coordinated with the weakest donor OMe uncoordinated. In non- or very weakly coordinating solvents there is strong evidence that the ligands coordinate in a tridentate fashion. Both Cu^{II} and Fe^{III} complexes exhibit highly reversible redox couples (Cu^{II}/Cu^I and Fe^{III}/Fe^{II}) pointing to high coordination flexibility for the ligands. Both the potentials of these redox couples and the EPR spectra (of powders, recrystallised samples and solutions) vary only slightly upon variation of the ligands. For the three crystallised complexes [Fe(OON1)Cl₂]₂, [Cu(OON1)Cl₂]_n and [Cu(OON3)Cl₂]₂ both enantiomers of the chiral ligands were found in the structures and very probably the chirality does not play a marked role in the spectroscopic and electrochemical results presented here. Detailed investigations on these complexes in the future will be devoted to this aspect. Also, the separation of the enantiomers and the investigation of their use

Table 6
Redox potentials of the Cu^{II} and Fe^{III} complexes.^a

Compound	$E_{1/2}$ (V)	Solvent
OON1	–3.23 irr. ^b	MeCN
OON2	–1.34 (65)	MeCN
OON3	–1.35 (61)	MeCN
[Cu(OON1)Cl ₂]	–0.17 (81)	THF
[Cu(OON2)Cl ₂]	–0.15 (78)	THF
[Cu(OON3)Cl ₂]	–0.10 (79)	THF
[Fe(OON1)Cl ₃]	–0.39 (83)	MeCN
[Fe(OON3)Cl ₃]	–0.30 (80)	MeCN
[Fe(OON1)Cl ₂] ₂	–1.36 (85) ^c	MeCN/DMF

^a From cyclic voltammetry in solvent/¹⁸Bu₄NPF₆ mixtures; potentials in V vs. FeCp₂/FeCp₂⁺, peak-to-peak separation in parenthesis.

^b Irreversible reduction, given is the cationic peak potential in V.

^c An additional minor reversible reduction wave is observed at –0.34 V resulting presumably from a mononuclear species from dissociation.

in catalysis will be attempted. Surprisingly, the ligands OON2 and OON3 exhibit reversible reduction waves at moderately negative potentials, while the ligand OON1 and all metal complexes exhibit irreversible reduction behaviour with very negative potentials. Although the generated reduced species could be studied by UV–Vis and EPR spectroelectrochemistry, this interesting phenomenon also requires some more investigations to allow an explanation.

4. Experimental

4.1. Instrumentation

Elemental analyses were carried out using a HEKAtech CHNS EuroEA 3000 Analyzer. UV–Vis–NIR absorption spectra were measured on Varian Cary50 Scan or Shimadzu UV-3600 photo spectrometers. EPR spectra were recorded in the X-band on a Bruker System ELEXSYS 500E equipped with a Bruker Variable Temperature Unit ER 4131VT. *g* values were calibrated using a dpph sample. Electrochemical experiments were carried out in 0.1 M *n*Bu₄NPF₆ solutions using a three-electrode configuration (glassy carbon electrode, Pt counter electrode, Ag/AgCl reference) and an Autolab PGSTAT30 potentiostat and function generator. The ferrocene/ferrocenium (FeCp₂/FeCp₂⁺) couple served as internal reference. Spectroelectrochemical UV–Vis experiments were performed using a THF/*n*Bu₄NPF₆ solution of OON3. The ligand radical anion for EPR experiments were generated using a THF solution of OON3 and reducing under Argon with potassium/cryptand [2.2.2].

4.2. Single crystal X-ray diffraction

Crystal structure determinations were performed at 293(2) K using graphite-monochromatised Mo K α radiation ($\lambda = 0.71073$ Å) on a IPDS I (STOE and Cie.). The structures were solved by direct methods (SHELXS-97) [20] and refined by full-matrix least-squares techniques against F^2 (SHELXL-97) [21]. The numerical absorption corrections (X-RED V1.22; Stoe & Cie, 2001) were performed after optimising the crystal shapes using X-SHAPE V1.06 (Stoe & Cie, 1999) [22]. The non-hydrogen atoms were refined with anisotropic displacement parameters without any constraints. All H atoms of the free ligands including the OH group were found during the refinement process.

4.3. XAS measurements

XAS measurements were performed at beamline X1 at the Hamburger Synchrotron Strahlungslabor (HASYLAB) under ambient conditions. A Si(1 1 1) double crystal monochromator was used for measurements at the Fe (7.112 keV) and Cu K-edge (8.979 keV). The second monochromator crystal was tilt for optimal harmonic rejection. The energy resolution for the Cu K-edge energy is estimated to 1.0 eV. The spectra were recorded in transmission mode with ionisation chambers filled with nitrogen. The individual pressures were adjusted to optimise the signal to noise ratio. Energy calibration was performed with an iron or copper metal foil, respectively, which was measured simultaneously with the samples between the second and third ionisation chamber. To avoid errors in the XANES region due to small changes in the energy calibration between two measurements, all spectra were calibrated to the edge position of the copper foil. The solid samples were embedded in an oxygen free cellulose matrix and pressed into pellets.

Data evaluation started with background absorption removal from the experimental absorption spectrum by subtracting a Victoreen-type polynomial. Due to several inflection points in the absorption edge, the threshold energy E_0 was determined

consistently by taking the energy at half the edge jump [23]. To determine the smooth part of the spectrum, corrected for pre-edge absorption, a piecewise polynomial was used. It was adjusted in such a way that the low-*R* components of the resulting Fourier transform were minimal. After division of the background-subtracted spectrum by its smooth part, the photon energy was converted to photoelectron wave numbers *k*. The resulting $\chi(k)$ -function was weighted with k^3 and Fourier transformed using a Hanning window function. Data analysis was performed in *k*-space with Fourier filtered data. The filtered range was chosen according to the range of significant data and is given in table A together with the results of the fitting procedure. Adjustment of the common theoretical EXAFS expression

$$\chi(k) = \sum_j \frac{N_j}{kr_j^2} S_0^2(k) F_j(k) e^{-2k^2\sigma_j^2} e^{-2r_j/\lambda} \sin[2kr_j + \delta_j(k)] \quad (2)$$

(N_j : one type of neighbour atoms *j* in a shell; r_j : distance of atoms *j* from the X-ray absorbing atom; S_0^2 : amplitude reduction factor; F_j : backscattering amplitude; σ^2 : Debye–Waller like factor; δ_j : overall phase shift) according to the curved wave formalism of the EXCURV98 program with XALPHA phase and amplitude functions [24]. The mean free path of the scattered electrons was calculated from the imaginary part of the potential (VPI set to -4.00 eV). An inner potential correction E_f was introduced when fitting experimental data with theoretical models that accounts for an overall phase shift between the experimental and calculated spectra.

In the fitting procedure, it was taken into account that the number of fitted parameters (N_{pars}) did not exceed the degrees of freedom (N_{ind}) which are calculated according to $N_{\text{ind}} = (2\Delta k\Delta R/\pi)$ [25]. The quality of fit is given in terms of the *R*-factor according to [26].

$$R = \sum_i \frac{k^3 |\chi^{\text{exp}}(k_i) - \chi^{\text{theo}}(k_i)|}{k^3 |\chi^{\text{exp}}(k_i)|} \cdot 100\% \quad (3)$$

4.4. Materials

4.4.1. 2-(Methoxy(pyridin-2-yl)methyl)phenol (OON1)

0.41 g (17.02 mmol, 2 eq) Mg was suspended in 20 mL dry diethyl ether and 1.67 mL (3.0 g, 12.77 mmol, 1.5 eq) 2-iodomethoxybenzene in 20 mL dry diethyl ether were added slowly. The reaction mixture was heated to 50–60 °C until it was brown and turbid (~45 min). Then 0.91 g (8.5 mmol, 1 eq) pyridin-2-carboxaldehyde was added drop by drop and the mixture became orange. After stirring overnight, 50 mL of water was slowly added to the reaction mixture. After phase separation and extraction of the aqueous phase with diethyl ether the combined organic phases were dried over Na₂SO₄. The solvent was then removed under vacuum and the remaining solid was washed with a small portion of acetone to yield 0.95 g (4.4 mmol, 52%) of an off-white powder. ¹H NMR ([D₆]-acetone): 8.50 H_{py6}, 1H, d; 7.69 H_{py4}, 1H, t; 7.40 H_{phen4/6}, 2H, t; 7.22 H_{py3/5}, 2H, m; 6.98 H_{phen3}, 1H, d; 6.92 H_{phen5}, 1H, t; 6.20 H_{methanol}, 1H, s; 5.33 OH, 1H, s; 3.83 OMe, 3H, s. ¹³C NMR (acetone-*d*₆): 162 C_{py2}, 1C, s; 157 C_{phen2}, 1C, s; 148 C_{py6}, 1C, d; 137 C_{py4}, 1C, d; 132 C_{phen1}, 1C, s; 128 C_{py3}, 1C, d; 127 C_{phen6}, 1C, d; 122 C_{py5}, 1C, d; 121 C_{phen4}, 1C, d; 120 C_{phen5}, 1C, d; 110 C_{phen3}, 1C, d; 69 C_{methanol}, 1C, d; 55 OMe1, 1C, q. Elemental Anal. Calc. for C₁₃H₁₃O₂N; M = 215.25 g mol⁻¹: C, 72.54; H, 6.09; N, 6.51. Found: C, 73.45; H, 6.04; N, 6.46%.

4.4.2. 2-(Methoxy(pyridin-2-yl)ethyl)phenol (OON2)

2.78 mL 2-iodo methoxybenzene (5 g, 21 mmol, 1 eq) and 0.61 g (25 mmol, 1.2 eq) Mg were reacted in dry THF to give the corresponding Grignard reagent. To this 2.75 mL (2.54 g, 21 mmol, 1 eq) 2-acetylpyridine were added drop by drop and the reaction

mixture was stirred for 16 h at 298 K. Then 100 mL of water was added and the resulting phases were separated. The aqueous phase was extracted with diethyl ether, the combined organic phases were dried over Na_2SO_4 and then the solvent was removed under vacuum to yield a brown oil. After a few hours big colourless crystals were formed and were separated by filtration and washing with cold acetone. Yield: 3.0 g (13 mmol, 64%) ^1H NMR ($[\text{D}_6]$ -acetone): 8.42 $\text{H}_{\text{py}6}$, 1H, d; 7.71 $\text{H}_{\text{py}4}$, 1H, t; 7.65 $\text{H}_{\text{py}3}$, 1H, d; 7.53 $\text{H}_{\text{phen}6}$, 1H, d; 7.23 $\text{H}_{\text{phen}4}$, 1H, t; 7.18 $\text{H}_{\text{py}5}$, 1H, t; 6.96 $\text{H}_{\text{phen}3}$, 1H, t; 6.90 $\text{H}_{\text{phen}5}$, 1H, d; 5.09 OH 1H, s; 3.55 OMe, 3H, s; 1.86 Me, 3H, s. ^{13}C NMR (acetone- d_6): 168 $\text{C}_{\text{phen}1}$, 1C, s; 158 $\text{C}_{\text{py}2}$, 1C, s; 148 $\text{C}_{\text{phen}2}$, 1C, s; 147 $\text{C}_{\text{py}6}$, 1C, d; 136 $\text{C}_{\text{py}4}$, 1C, d; 128 $\text{C}_{\text{phen}4}$, 1C, d; 127 $\text{C}_{\text{py}3}$, 1C, d; 121 $\text{C}_{\text{py}5}$, 1C, d; 120 $\text{C}_{\text{phen}5/6}$, 2C, d; 112 $\text{C}_{\text{phen}3}$, 1C, d; 76 C_{OH} , 1C, s; 55 $\text{C}_{\text{phen}2}$, 1C, q; 28 C_{Me} , 1C, q. Elemental Anal. Calc. for $\text{C}_{14}\text{H}_{15}\text{O}_2\text{N}$; $M = 229.27 \text{ g mol}^{-1}$: C, 73.34; H, 6.59; N, 6.11. Found: C, 73.23; H, 6.54; N, 6.06%.

4.4.3. 2-(Methoxy(pyridin-2-yl)benzyl)phenol (OON3)

2.78 mL 2-iodo methoxybenzene (5 g, 21 mmol, 1 eq) and 612 mg (25 mmol, 1.2 eq) Mg were reacted in 30 mL dry THF to give the corresponding Grignard reagent. To this 3.84 g (21 mmol, 1 eq) benzoylpyridine were added slowly. The reaction mixture was stirred overnight at 298 K. Then 50 mL water was slowly added and the resulting phases were separated. The aqueous phase was extracted with diethyl ether, the combined organic phases were dried over Na_2SO_4 and the solvent was removed under vacuum. The crude product, a colourless solid, was recrystallised from acetone to yield 5.4 g (15 mmol, 72%) of colourless crystals. ^1H NMR ($[\text{D}_6]$ -acetone): 8.46 $\text{H}_{\text{py}6}$, 1H, d; 7.76 $\text{H}_{\text{py}4}$, 1H, t; 7.59 $\text{H}_{\text{py}3}$, 1H, d; 7.39 $\text{H}_{\text{benz}2/6}$, 2H, d; 7.27 $\text{H}_{\text{benz}3/4/5/\text{phen}4/\text{py}5}$, 5H, m; 6.99 $\text{H}_{\text{phen}3}$, 1H, d; 6.95 $\text{H}_{\text{phen}6}$, 1H, d; 6.85 $\text{H}_{\text{phen}5}$, 1H, t; 5.67 OH 1H, s; 3.49 OMe, 3H, s; ^{13}C NMR (acetone- d_6): 167 $\text{C}_{\text{py}2}$, 1C, s; 159 $\text{C}_{\text{phen}1}$, 1C, s; 147 $\text{C}_{\text{benz}1}$, 1C, s; 148 $\text{C}_{\text{py}6}$, 1C, d; 137 $\text{C}_{\text{py}4}$, 1C, d; 130 $\text{C}_{\text{phen}6}$, 1C, d; 128 $\text{C}_{\text{benz}2/6/\text{phen}4}$, 3C, d; 127 $\text{C}_{\text{benz}3/4/5}$, 3C, d; 123 $\text{C}_{\text{py}3/5}$, 2C, d; 121 $\text{C}_{\text{phen}5}$, 1C, d; 121 $\text{C}_{\text{phen}1}$, 1C, s; 113 $\text{C}_{\text{phen}3}$, 1C, d; 82 C_{OH} , 1C, s; 56 $\text{C}_{\text{phen}2}$, 1C, q. Elemental Anal. Calc. for $\text{C}_{19}\text{H}_{17}\text{O}_2\text{N}$; $M = 365.57 \text{ g mol}^{-1}$: C, 78.33; H, 5.88; N, 4.81. Found: C, 78.14; H, 6.01; N, 5.01%.

4.4.4. General procedure for the synthesis of the complexes

1 eq of the OON-ligand was dissolved in methanol and 1 eq of the metal chloride (MCl_2 or MCl_3 , respectively), dissolved in methanol/acetone (1:1) was added. The mixture was stirred at 298 K for 14 h. The solvent was removed under reduced pressure and the remaining solids were washed with cold acetone.

4.4.5. $[\text{Zn}(\text{OON}1)\text{Cl}_2]$

100 mg (0.46 mmol, 1 eq) of OON1 were reacted with 79 mg (0.46 mmol, 1 eq) of anhydrous ZnCl_2 to yield 160 mg (0.45 mmol, 97%) of a colourless powder. NMR (300 MHz, $[\text{D}_6]$ -acetone): ^1H : 8.77 (s, 1H, H_{OH}), 8.76 (d, 1H, $\text{H}_{6\text{Py}}$), 8.12 (t, 1H, $\text{H}_{4\text{Py}}$), 7.71 (t, 1H, $\text{H}_{5\text{Py}}$), 7.48 (d, 1H, $\text{H}_{6\text{Ph}}$), 7.48 (d, 1H, $\text{H}_{3\text{Py}}$), 7.39 (t, 1H, $\text{H}_{4\text{Ph}}$), 7.11 (d, 1H, $\text{H}_{3\text{Ph}}$), 6.97 (t, 1H, $\text{H}_{5\text{Ph}}$), 6.75 (s, 1H, $\text{H}_{\text{methanol}}$), 3.84 (s, 3H, H_{OMe}). Elemental Anal. Calc. for $\text{C}_{13}\text{H}_{13}\text{O}_2\text{NCl}_2\text{Zn}$; $M = 351.54 \text{ g mol}^{-1}$: N, 3.98; C, 44.42; H, 3.73. Found: N, 3.81; C, 43.20; H, 3.71%.

4.4.6. $[\text{Zn}(\text{OON}2)\text{Cl}_2]$

100 mg (0.44 mmol, 1 eq) OON2 and 59 mg (0.44 mmol, 1 eq) of anhydrous ZnCl_2 were reacted to yield 101 mg (0.28 mmol, 64%) of a colourless powder. NMR (300 MHz, $[\text{D}_6]$ -acetone): ^1H : 8.70 (d, 1H, $\text{H}_{6\text{Py}}$), 8.02 (t, 1H, $\text{H}_{4\text{Py}}$), 7.94 (s(br), 1H, H_{OH}), 7.76 (d, 1H, $\text{H}_{6\text{Ph}}$), 7.63 (t, 1H, $\text{H}_{5\text{Py}}$), 7.23 (d, 1H, $\text{H}_{3\text{Py}}$), 7.43 (t, 1H, $\text{H}_{4\text{Ph}}$), 7.08 (t, 1H, $\text{H}_{5\text{Ph}}$), 6.99 (d, 1H, $\text{H}_{3\text{Ph}}$), 3.49 (s, 3H, H_{OMe}), 2.08 (s, 3H, H_{Me}). Elemental Anal. Calc. for $\text{C}_{14}\text{H}_{15}\text{O}_2\text{NCl}_2\text{Zn}$; $M = 365.57 \text{ g mol}^{-1}$: N, 3.83; C, 46.00; H, 4.14. Found: N, 3.90; C, 44.91; H, 4.23%.

4.4.7. $[\text{Zn}(\text{OON}3)\text{Cl}_2]$

100 mg (0.34 mmol, 1 eq) OON3 and 46 mg (0.34 mmol, 1 eq) of anhydrous ZnCl_2 were reacted to yield 104 mg (0.24 mmol, 71%) of a colourless powder. NMR (300 MHz, $[\text{D}_6]$ -acetone): ^1H : 8.73 (d, 1H, $\text{H}_{6\text{Py}}$), 8.07 (t, 1H, $\text{H}_{4\text{Py}}$), 7.65 (t, 1H, $\text{H}_{5\text{Py}}$), 7.43 (t, 1H, $\text{H}_{4\text{Ph}}$), 7.34 (m, 6H, $\text{H}_{2,3,4,5,6\text{Bnz}}$), 7.14 (m, 2H, $\text{H}_{5,6\text{Ph}}$), 6.91 (d, 1H, $\text{H}_{3\text{Ph}}$), 6.72 (s, 1H, H_{OH}), 3.66 (s, 3H, H_{OMe}). Elemental Anal. Calc. for $\text{C}_{19}\text{H}_{17}\text{O}_2\text{NCl}_2\text{Zn}$; $M = 427.64 \text{ g mol}^{-1}$: N, 3.28; C, 53.36; H, 4.01. Found: N, 3.15; C, 52.09; H, 4.04%.

4.4.8. $[\text{Cu}(\text{OON}1)\text{Cl}_2]$

220 mg (1 mmol, 1 eq) OON1 were reacted with 138 mg (1 mmol, 1 eq) of anhydrous CuCl_2 to yield 283 mg (0.81 mmol, 81%) of a green solid. Elemental Anal. Calc. for $\text{C}_{13}\text{H}_{13}\text{O}_2\text{NCl}_2\text{Cu}$; $M = 349.70 \text{ g mol}^{-1}$: N, 4.01; C, 44.65; H, 3.75. Found: N, 3.88; C, 45.21; H 3.89%.

4.4.9. $[\text{Cu}(\text{OON}2)\text{Cl}_2]$

100 mg (0.44 mmol, 1 eq) OON2 were reacted with 59 mg (0.44 mmol, 1 eq) of anhydrous CuCl_2 to yield 107 mg (0.29 mmol, 66%) of a green solid. Elemental Anal. Calc. for $\text{C}_{14}\text{H}_{15}\text{O}_2\text{NCl}_2\text{Cu}$; $M = 363.73 \text{ g mol}^{-1}$: N, 3.85; C, 46.23; H, 4.16. Found: N, 3.97; C, 47.92; H, 4.26.

4.4.10. $[\text{Cu}(\text{OON}3)\text{Cl}_2]$

100 mg (0.34 mmol, 1 eq) OON3 were reacted with 46 mg (0.34 mmol, 1 eq) of anhydrous CuCl_2 to yield 103 mg (0.24 mmol, 71%) of a green solid. Elemental Anal. Calc. for $\text{C}_{19}\text{H}_{16}\text{O}_2\text{NCl}_2\text{Cu}$; $M = 424.79 \text{ g mol}^{-1}$: N, 3.30; C, 53.72; H, 3.80. Found: N, 3.27; C, 52.99; H, 3.73%.

4.4.11. $[\text{Ni}(\text{OON}1)\text{Cl}_2]$

100 mg (0.46 mmol, 1 eq) OON1 were reacted with 110 mg (0.46 mmol, 1 eq) $\text{NiCl}_2 \cdot 6\text{H}_2\text{O}$ to yield 60 mg (0.17 mmol, 37%) of a green solid. NMR (300 MHz, $[\text{D}_6]$ -acetone): ^1H : 11.46; 7.70; 7.46; 7.20; 6.94; 6.80; 5.38; 4.80; 4.28; 3.83 ppm. Elemental Anal. Calc. for $\text{C}_{13}\text{H}_{13}\text{O}_2\text{NCl}_2\text{Ni}$; $M = 344.85 \text{ g mol}^{-1}$: N, 4.06; C, 45.28; H, 3.80. Found: N, 3.88; C, 43.72; H, 3.98%.

4.4.12. $[\text{Ni}(\text{OON}2)\text{Cl}_2]$

100 mg (0.43 mmol, 1 eq) OON2 were reacted with 102 mg (0.43 mmol, 1 eq) $\text{NiCl}_2 \cdot 6\text{H}_2\text{O}$ to yield 74 mg (0.21 mmol, 49%) of a green solid. NMR (300 MHz, $[\text{D}_6]$ -acetone): ^1H : 15.49; 13.27; 8.42; 7.51; 6.95; 5.52; 4.49; 2.00 ppm. Elemental Anal. Calc. for $\text{C}_{14}\text{H}_{15}\text{O}_2\text{NCl}_2\text{Ni}$; $M = 356.98 \text{ g mol}^{-1}$: N, 3.90; C, 46.85; H, 4.21. Found: N, 4.09; C, 44.52; H, 4.05%.

4.4.13. $[\text{Ni}(\text{OON}3)\text{Cl}_2]$

100 mg (0.34 mmol, 1 eq) OON3 were reacted with 82 mg (0.34 mmol, 1 eq) $\text{NiCl}_2 \cdot 6\text{H}_2\text{O}$ to yield 84 mg (0.20 mmol, 59%) of a green solid. NMR (300 MHz, $[\text{D}_6]$ -acetone): ^1H : 14.10; 8.12; 7.47; 6.93; 4.60; 3.54 ppm. Elemental Anal. Calc. for $\text{C}_{19}\text{H}_{17}\text{O}_2\text{NCl}_2\text{Ni}$; $M = 420.94 \text{ g mol}^{-1}$: N, 3.33; C, 54.21; H, 4.07. Found: N, 3.39; C, 52.85; H, 4.24%.

4.4.14. $[\text{Fe}(\text{OON}1)\text{Cl}_3]$

100 mg (0.46 mmol, 1 eq) OON1 were reacted with 92 mg (0.46 mmol, 1 eq) $\text{FeCl}_3 \cdot 6\text{H}_2\text{O}$ to yield 157 mg (0.42 mmol, 91%) of a dark red solid. Elemental Anal. Calc. for $\text{C}_{13}\text{H}_{13}\text{O}_2\text{NCl}_3\text{Fe}$; $M = 377.45 \text{ g mol}^{-1}$: N, 3.71; C, 41.37; H, 3.47. Found: N, 3.84; C, 42.67; H, 3.56%.

4.4.15. $[\text{Fe}(\text{OON}1)\text{Cl}_2]_2$

50 mg (0.13 mmol, 2 eq) $[\text{FeCl}_3(\text{OON}1)]$ were dissolved in acetone and stirred for 60 h. A dark red precipitate was formed and filtered off. After washing with acetone 37 mg (0.05 mmol, 92%) were

obtained. *Anal. Calc.* for $C_{26}H_{24}O_4N_2Cl_6Fe_2$; $M = 681.98 \text{ g mol}^{-1}$; N, 3.55; C, 45.79; H, 4.11. Found: N, 4.06; C, 44.68; H, 3.46%.

4.4.16. $[Fe(OON2)Cl_x]_y$

170 mg (0.74 mmol, 1 eq) OON2 were reacted with 148 mg (0.74 mmol, 1 eq) $FeCl_3 \cdot 6H_2O$ to yield 253 mg of a bright orange solid. The product is presumably polymeric, contains more than one Fe^{III} species (EPR spectroscopy) and the exact stoichiometry of this compound could not be determined. Elemental *Anal.* found: N, 3.07; C, 49.66; H, 3.75%.

4.4.17. $[Fe(OON3)Cl_3]$

100 mg (0.34 mmol, 1 eq) OON3 were reacted with 68 mg (0.34 mmol, 1 eq) $FeCl_3 \cdot 6H_2O$ to yield 124 mg (0.27 mmol, 79%) of a brown-red solid. Elemental *Anal. Calc.* for $C_{19}H_{17}O_2NCl_3Fe$; $M = 453.55 \text{ g mol}^{-1}$; N, 3.09; C, 50.32; H, 3.78. Found: N, 3.07; C, 49.66; H, 3.75%.

4.4.18. $[Fe(OON1)Cl_2]$

100 mg (0.46 mmol, 1 eq) OON1 were reacted with 93 mg (0.46 mmol, 1 eq) $FeCl_2 \cdot 4H_2O$ to yield 140 mg (0.41 mmol, 89%) of an orange-brown solid. Elemental *Anal. Calc.* for $C_{13}H_{13}O_2NCl_2Fe$; $M = 342.00 \text{ g mol}^{-1}$; C, 45.65; H, 3.83; N, 4.10. Found: C, 47.87; H, 3.56; N, 4.02%.

4.4.19. $[Fe(OON2)Cl_2]$

94 mg (0.41 mmol, 1 eq) OON2 and 82 mg (0.41 mmol, 1 eq) $FeCl_2 \cdot 4H_2O$ were dissolved in 5 mL methanol each. Both solutions were combined and stirred for 6 h at room temperature. During this time an intensive coloured, orange precipitate was formed, which was filtered off and washed with three portions of cold methanol to yield 139 mg (0.39 mmol, 95%). Elemental *Anal. Calc.* for $C_{14}H_{15}O_2NCl_2Fe$; $M = 356.03 \text{ g mol}^{-1}$; C, 47.23; H, 4.25; N, 3.93. Found: C, 48.65; H, 4.20; N, 3.98%.

4.4.20. $[Fe(OON3)Cl_2]$

97 mg (0.33 mmol, 1 eq) OON3 and 66 mg (0.33 mmol, 1 eq) $FeCl_2 \cdot 4H_2O$ were dissolved in 5 mL methanol each. Both solutions were combined and stirred for 6 h at room temperature. The solvent of the resulting orange-brown solution was removed under vacuum to yield 83 mg (0.20 mmol, 61%) of a brown powder. Elemental *Anal. Calc.* for $C_{19}H_{17}O_2NCl_2Fe$; $M = 418.09 \text{ g mol}^{-1}$; C, 54.58; H, 4.10; N, 3.35. Found: C, 53.88; H, 3.92; N, 3.45.

Acknowledgments

We would like to thank Dr. Ingo Pantenburg and Ingrid Müller from the Institute for Inorganic Chemistry for the X-ray measurements and the "Studienstiftung des Deutschen Volkes" for financial support (KB). Dr. Eric J. L. McInnes, School of Chemistry, The University of Manchester, UK is acknowledged for helpful comments..

Appendix A. Supplementary material

CCDC 801045–801049 contain the supplementary crystallographic data for this paper. These data can be obtained free of charge from The Cambridge Crystallographic Data Centre via www.ccdc.cam.ac.uk/data_request/cif. Supplementary data associated with this article can be found, in the online version, at doi:10.1016/j.ica.2011.02.072.

References

- [1] (a) J.T. Singleton, *Tetrahedron* 59 (2003) 1837;
(b) M.E. van der Boom, D. Milstein, *Chem. Rev.* 103 (2003) 1759;

- (c) J.M. Hawkins, K.B. Sharpless, *Tetrahedron Lett.* 28 (1987) 2825;
(d) M. Albrecht, G. van Koten, *Angew. Chem. Int. Ed.* 40 (2001) 3750.
[2] (a) J.A. Thich, C.C. Ou, D. Powers, B. Vasiliou, D. Mastropaolo, J.A. Potenza, H.J. Schugar, *J. Am. Chem. Soc.* (1976) 1425;
(b) P.A. Brayshaw, J.-C.G. Bünzli, P. Froidevaux, J.M. Harrowfield, Y. Kim, A.N. Sobolev, *Inorg. Chem.* 34 (1995) 2068;
(c) F. Renaud, C. Piguët, G. Bernardinelli, J.-C.G. Bünzli, G. Hopfgartner, *J. Am. Chem. Soc.* 121 (1999) 9326.
[3] R. Castarlenas, M.A. Esteruelas, E. Onate, *Organometallics* 26 (2007) 3082.
[4] (a) M. Melnik, C.E. Holloway, *J. Coord. Chem.* 49 (1999) 69;
(b) R.M. Gauvin, J.A. Osborn, J. Kress, *Organometallics* 19 (2000) 2944;
(c) E. Gómez, V. Santes, V. de la Luz, N. Farfán, *J. Organomet. Chem.* 622 (2001) 54.
[5] (a) K.V. Zaitsev, M.V. Bermeshev, S.S. Karlov, Y.F. Oprunenko, A.V. Churakov, J.A.K. Howard, G.S. Zaitseva, *Inorg. Chim. Acta* 360 (2007) 2507;
(b) R. Fandos, B. Gallego, A. Otero, A. Rodriguez, M.J. Ruiz, P. Terreros, C. Pastor, *Organometallics* 26 (2007) 2896;
(c) R.J. Fites, A.T. Yeager, T.L. Sarvela, W.A. Howard, G. Zhu, K. Pang, *Inorg. Chim. Acta* 359 (2006) 248;
(d) J.M. Berg, R.H. Holm, *Inorg. Chem.* 22 (1983) 1768.
[6] (a) C. Boskovic, W. Wernsdorfer, K. Foltz, J.C. Huffman, D.N. Hendrickson, G. Christou, *Inorg. Chem.* 41 (2002) 5107;
(b) J. Yoo, E.K. Brechin, A. Yamaguchi, M. Nakano, J.C. Huffman, A.L. Maniero, L.-C. Brunel, K. Awaga, H. Ishimoto, G. Christou, D.N. Hendrickson, *Inorg. Chem.* 39 (2000) 3615;
(c) E.K. Brechin, J. Yoo, M. Nakano, J.C. Huffman, D.N. Hendrickson, G. Christou, *Chem. Commun.* (1999) 783.
[7] (a) V.T. Yilmaz, S. Güney, O. Andac, W.T.A. Harrison, *J. Coord. Chem.* 56 (2003) 21;
(b) O. Andac, S. Güney, Y. Topcu, V.T. Yilmaz, W.T.A. Harrison, *Acta Crystallogr., Sect. C* 58 (2002) m17;
(c) S. Winter, W. Seichter, E. Weber, *J. Coord. Chem.* 57 (2004) 997;
(d) S. Winter, W. Seichter, E. Weber, *Z. Anorg. Allg. Chem.* 630 (2004) 434;
(e) M. Koman, M. Melnik, *Polyhedron* 16 (1997) 2721;
(f) M. Melnik, M. Koman, L. Macaskova, T. Glowiak, R. Grobelny, J. Mrozinsky, *J. Coord. Chem.* 43 (1998) 159;
(g) M. Koman, M. Melnik, J. Moncol, *Inorg. Chem. Commun.* 3 (2000) 262.
[8] A.K. Gupta, J. Kim, *Acta Crystallogr., Sect. C* 59 (2003) m262.
[9] (a) J.A. Davies, F.R. Hartley, *Chem. Rev.* 81 (1981) 79;
(b) R.G. Pearson, *Inorg. Chem.* 27 (1988) 734;
(c) R.G. Pearson, *J. Am. Chem. Soc.* 85 (1963) 3533.
[10] A. Klein, S. Elmas, K. Butsch, *Eur. J. Inorg. Chem.* (2009) 2271.
[11] (a) T. Kawato, H. Koyama, H. Kanatomi, Y. Muramoto, *Inorg. Chim. Acta* 183 (1991) 107;
(b) F.D. Rochon, A.L. Beauchamp, C. Bensimon, *Can. J. Chem.* 74 (1996) 2121.
[12] A. Klein, K. Butsch, J. Neudörfl, *Inorg. Chim. Acta* 363 (2010) 3282.
[13] A. Klein, K. Butsch, S. Elmas, D. Heift, S. Nitsche, I. Schlipf, H. Bertagnolli, *Polyhedron*, submitted for publication.
[14] J.C. Wilson, P.D. Verweij, W.L. Driessen, J. Reedijk, *Inorg. Chim. Acta* 192 (1992) 219.
[15] G.J.A.A. Koolhaas, W.L. Driessen, P.J. Van Koningsbruggen, J. Reedijk, A.L. Spek, *J. Chem. Soc., Dalton Trans.* (1993) 3803.
[16] C.-D. Zhang, S.-X. Liu, C.-Y. Sun, F.-J. Ma, Z.-M. Su, *Cryst. Growth Des.* 9 (2009) 3655.
[17] R. Viswanathan, M. Palaniandavar, T. Balasubramanian, P.T. Muthiah, *J. Chem. Soc., Dalton Trans.* (1996) 2519.
[18] C. Reichardt, *Angew. Chem.* 1 (1965) 30.
[19] (a) N.I. Tzerpos, A.K. Zarkadis, R.P. Kreher, L. Repas, M. Lehnig, *J. Chem. Soc., Perkin Trans. 2* (1995) 755;
(b) D. Dünnebacke, W.P. Neumann, A. Penenory, U. Stewen, *Ber.* (1988) 533;
(c) M. Ando, S. Yoshiike, T. Suzuki, T. Ichimura, T. Okutsu, M. Ueda, H. Horiuchi, H. Hiratsuka, A. Kawai, K. Shibuya, *J. Photochem. Photobiol. A: Chem.* 174 (2005) 194.
[20] (a) G.M. Sheldrick, *Acta Cryst. A* (2008) 112;
(b) G.M. Sheldrick, *SHELX-97*, Programs for Crystal Structure Analysis, Göttingen, 1997;
(c) L.J. Farrugia, *J. Appl. Cryst.* 32 (1999) 837.
[21] G.M. Sheldrick, *SHELXL-97*, Program for the Refinement of Crystal Structures, Universität Göttingen, 1997.
[22] [a] STOE X-RED, Data Reduction Program, Version 1.22/Windows, STOE & Cie, Darmstadt, 2001;
[b] STOE X-SHAPE, Crystal Optimisation for Numerical Absorption Correction, Version 1.06/Windows, STOE & Cie, Darmstadt, 1999.
[23] (a) T.S. Ertel, H. Bertagnolli, S. Hückmann, U. Kolb, D. Peter, *Appl. Spectrosc.* 46 (1992) 690;
(b) M. Newville, P. Livins, Y. Yacoby, J.J. Rehr, E.A. Stern, *Phys. Rev. B* 47 (1993) 14126.
[24] S.J. Gurman, N. Binsted, I. Ross, *J. Phys. C* 17 (1984) 143.
[25] E.A. Stern, *Phys. Rev. B* 48 (1993) 9825.
[26] N. Binsted, in: F. Mosselman (Ed.), EXCURV98, CCLRC Daresbury Laboratory Computer Program, Manual, 1998.